Device

Article

Transistor-like triboiontronics with record-high charge density for self-powered sensors and neurologic analogs

Graphical abstract

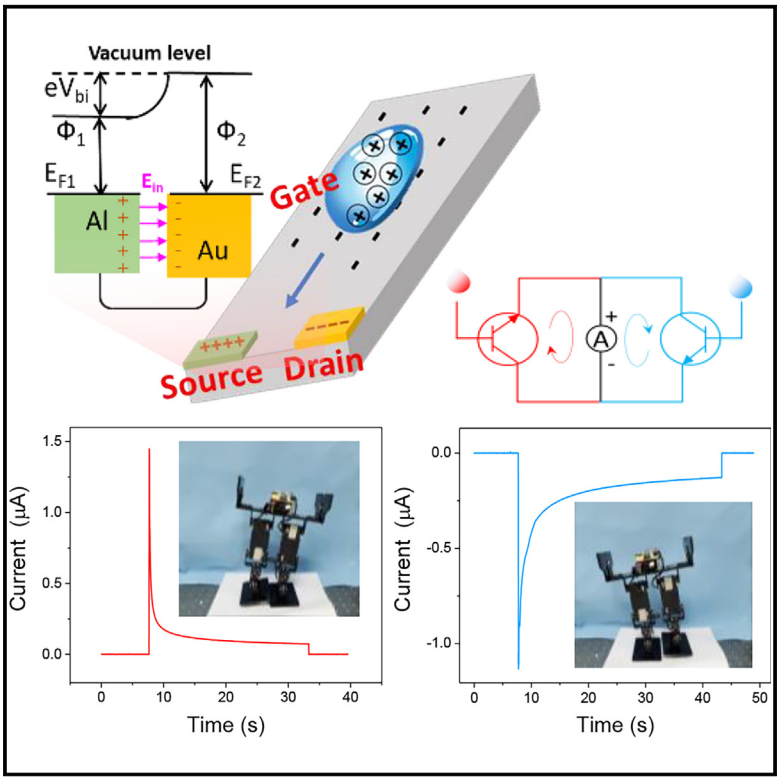

Highlights

- A direct current was realized for triboelectrification and work function difference
- Triboiontronics with record-high charge density (13.9 mC/m^2) was realized
- Self-powered sensors with high signal-to-noise were enabled by TTI
- A mechano-driven neurologic circuit was built by TTI to control robotic movements

Authors

Shaoxin Li, Zhiwei Zhang, Feiyao Yang, ..., Morten Willatzen, Zhong Lin Wang, Di Wei

Correspondence

zhong.wang@mse.gatech.edu (Z.L.W.), weidi@binn.cas.cn (D.W.)

In brief

Gated by the water droplet, two different metals were analogous to the source and drain terminals to form TTIs capable of rectifying and switching the output current without external voltage. A neurologic circuit to control robotic movements was also built by TTI. We envision that triboiontronics will provide a new paradigm for futuristic low-power, in-sensor computing and neuromorphic analogs.

Explore
Early prototypes with exciting performance and new methodology

Li et al., 2024, Device 2, 100332
June 21, 2024
https://doi.org/10.1016/j.device.2024.100332

CellPress

Device

CellPress
OPEN ACCESS

Article

Transistor-like triboiontronics with record-high charge density for self-powered sensors and neurologic analogs

Shaoxin Li,[1,2] Zhiwei Zhang,[1,2] Feiyao Yang,[1] Xiang Li,[1,2] Puguang Peng,[1,2] Yan Du,[1,2] Qixuan Zeng,[5] Morten Willatzen,[1,2] Zhong Lin Wang,[1,3,4,*] and Di Wei[1,6,*]

[1]Beijing Institute of Nanoenergy and Nanosystems, Chinese Academy of Sciences, Beijing 101400, P.R. China
[2]School of Nanoscience and Engineering, University of the Chinese Academy of Sciences, Beijing 100049, P.R. China
[3]Georgia Institute of Technology, Atlanta, GA 30332, USA
[4]Guangzhou Institute of Blue Energy, Knowledge City, Huangpu District, Guangzhou 510555, China
[5]College of Physics, Guizhou Province Key Laboratory for Optoelectronic Technology and Application, Guizhou University, Guiyang 550025, China
[6]Lead contact
*Correspondence: zhong.wang@mse.gatech.edu (Z.L.W.), weidi@binn.cas.cn (D.W.)
https://doi.org/10.1016/j.device.2024.100332

THE BIGGER PICTURE Despite recent advancements in electronic devices based on transistors, computers require an increasing number of electronic components and more energy consumption for information processing and data transmission, nearing the limit of Moore's law. Iontronics is an emerging technology that facilitates information logic circuits with an energy-efficient architecture, inspired by the function of neurons in biological systems. In this work, we used the ubiquitous solid-liquid triboelectrification effect to regulate iontronics and proposed transistor-like triboiontronics (TTI) by work function difference. TTI produced a recorded charge density, simultaneously demonstrating the capability to rectify and switch the output current without the need for external voltage. Such advantages of TTIs enabled self-powered threshold sensors with a higher signal-to-noise ratio and a controllable neurologic circuit.

SUMMARY

The transistor, as the basic unit of electronics based on von Neumann architecture, is approaching the limit of Moore's law in the era of big data. Inspired by the biological system, iontronics provides an energy-efficient architecture to transmit data. Here, we used the ubiquitous solid-liquid triboelectrification to regulate the output characteristics of iontronics and proposed transistor-like triboiontronics (TTI) by work function difference. Unlike previous studies, which scavenged induced electrostatic charges from a solid surface, the triboelectric charges of liquids were also captured here, creating a record-high charge density of 13.926 mC/m^2. Gated by the water droplet, TTI's gate-tunable function holds great significance for self-powered threshold sensors with high signal-to-noise ratio and enables a neurologic circuit to control robotic movements. We envision that triboiontronics will provide a new paradigm for futuristic in-sensor computing and neuromorphic analogs.

INTRODUCTION

The conventional von Neumann computing architecture in electronics is facing challenges with the end of Moore's law, and further shrinking transistors to the current technology limitation will require monumental efforts that are increasingly complex and energy consuming.[1,2] Inspired by the function of neurons in biological systems, iontronics is an emerging technology that enables the construction of neuromorphic logic circuits through combining electronic properties and ionic characteristics.[3,4] With the advantage of lower energy consumption for information processing, one goal of iontronics is to effectively rectify or switch the ionic current for computational or logic signal communication.[5–7] Efforts to regulate the ionic current had exclusively relied on the electromotive force generated from electrochemical redox reactions, salinity gradients, or external voltage, limiting signal response time by either reaction rate or durability. Most recently, iontronic diodes and transistors have also been realized by the built-in field from the electrical double layer (EDL) formed by two ionoelastomers of opposite polarity.[8] However, it is subject to elastomer deformation, which might be limited by material durability.

Please cite this article in press as: Li et al., Transistor-like triboiontronics with record-high charge density for self-powered sensors and neurologic analogs, Device (2024), https://doi.org/10.1016/j.device.2024.100332

The ubiquitous contact electrification (CE) at the solid and liquid interface, where its electron transfer process is closely related to the interfacial ionic migration, offers a new approach to tailor iontronics.[9–12] Generally, the triboelectric charges on the solid surface are scavenged through a triboelectric nanogenerator (TENG), which is an emerging tool to convert mechanical energy to electrical power.[13,14] The CE efficiency at the solid-liquid interface is a critical factor for effective energy conversion.[15] However, the inherent interface between the insulating solid dielectric and liquid inevitably limits the triboelectric charge transport to the external circuit, and some triboelectric energy stored in the water is wasted. Recently, droplet-based electricity generators (DEGs) were developed to generate high output power through the CE between water and a single electrode.[16–18] However, there is no complete loop inside such an architecture for triboelectric charge transport due to the micron-thick insulating solid dielectric. Thus, DEGs still need to be integrated with the external power management circuit, including additional rectification, conversion, and storage components, to convert alternating current (AC) into a direct current (DC) output. Although it is referred to as a transistor structure,[19] it does not show the function of switching electrical signals.

In this work, gate-tunable triboiontronics enabled by a water droplet with adjustable charge is proposed through synergy effects of triboelectrification and work function difference. A deionized (DI) water droplet was triboelectrically charged through friction against the insulating solid dielectrics, and its accumulated charges were discharged to the external circuit under the built-in electric field (E_{in}) from metal electrodes with different work functions. A DC output was generated due to the directional migration of ions in water droplets driven by E_{in}. As one type of iontronics, triboiontronics would have the benefits of not being affected by magnetic fields and offer broader applications than conventional electronics. Furthermore, serving the triboelectrically charged water droplet as a dynamic gate and two dissimilar electrodes as the source and drain terminals, transistor-like triboiontronics (TTI) was established, which enabled mechanical tuning of the amplitude and direction of the DC signal. With the advantage of the low interfacial resistance between metal and water and spontaneous electromotive force from E_{in}, the transferred charge density of a single droplet was increased to 13.926 mC/m^2, which was an order of magnitude higher than the best data reported so far (from 0.014 to 0.566 mC/m^2).[18,21–29] Therefore, TTI showed a fast self-powered threshold sensor capability with an excellent signal-to-noise ratio (SNR), which is especially suitable for alarm and warning systems for emergencies, such as shipwrecks, driving collisions, earthquakes, bridge/tunnel collapse, etc. It also promise for construction of a neurologic circuit to control robotic movements, implying its great potential for applications in futuristic neuromorphic circuits and in-sensor computing.

RESULTS AND DISCUSSION

Over 150 years ago, the charging effect between two materials from work function difference was thoroughly investigated by Lord Kelvin.[30] For example, the metals aluminum (Al) and gold (Au) share the same local vacuum level (E_v) and are electrically neutral before connecting (Figure 1Ai). Upon circuit connection, electrons flow from Al to Au until their Fermi levels are uniformly redistributed, forming E_{in} (Figure 1Aii). Although such a work function difference has been used to generate electrical power to the external circuit,[31–33] their output powers are too low to be applicable. Analogous to the rectification effect of a diode, here, the E_{in} from the work function difference between Al and Au was used as a junction to separate the positive and negative charges in the triboelectrically charged DI water droplet, establishing triboiontronics. As shown in Figure 1B, a DI water droplet (10 μL) was dragged by an Al plate electrode on the hydrophobic polytetrafluoroethylene (PTFE) surface (Figure S1A), and their contact area was about 12.57 mm^2. Such a triboelectrification process generated positive charges within the DI water droplet and negative charges on the surface of PTFE (Figure 1Bi magnified view). As shown in the COMSOL multiphysical model in Figure S2 and preset parameters in Table S1, the potential difference between Al and Au increased when the DI water slid from the left side to the right side of the PTFE surface (Figure 1C). The simulated results also indicated the triboelectric charging process of the DI water droplet, where positive charges were generated and accumulated when it slid on the PTFE surface, where the negative charges were gradually maintained. It caused the Al electrode potential to increase and produced an induction current (I_{e1}) in the external circuit. When the DI water droplet was transferred from the PTFE surface to Au electrode, its inner ionic charges migrated in one direction under the E_{in} between the Au and Al electrodes (Figure 1Bii). The charge transport to the external circuit was enhanced by the direct contact at the water-metal interface and the spontaneous electromotive force of E_{in}, compared with the multiple water-PTFE-metal interfaces based on conventional electrostatic induction. Therefore, a DC ionic current (I_i) (Figure 1C) was generated under E_{in}, which was two orders of magnitude higher than I_e (Figure 1D). The triboelectrification occurred again when the DI water droplet was dragged back to the PTFE surface, generating a reversed induction current (I_{e2}), as shown in (Figure 1Biii). Some positive charges of the DI water droplet might be absorbed on the surface of the Au electrode to form the EDL, which was similar to the depletion layer at a diode junction. After several reciprocating sliding processes (Figures 1Biv–1Bvi), the EDL formation became stable; thus, the migration of triboelectric charges in DI water under E_{in} produced a stable I_i (Figure 1Bvii). As shown in Figure 1D, the peak value of I_i reached up to 4.6 μA at an initial stage. It gradually decayed within 30 s and finally remained at about 0.3 μA. It can be seen in Figure 1E that the DC output voltage was about 0.6 V, and the I_i rectification effect between the Al and Au electrodes is shown in Figure S3. Moreover, the charge accumulation phenomenon of TTI can be seen in Figure 1F, and its charge density could reach 3.183 mC m^{-2} during each discharge stage under E_{in}.

To further prove the importance of triboelectrification and work function difference for high-performance triboiontronics, we designed parallel devices, as shown in Figures 2A and 2B. Since the PTFE blocked water from contacting the Al and Au electrodes, the output AC current was only 20 nA based on electrostatic induction (Figure 2A). When the DI water droplet

Please cite this article in press as: Li et al., Transistor-like triboiontronics with record-high charge density for self-powered sensors and neurologic analogs, Device (2024), https://doi.org/10.1016/j.device.2024.100332

CellPress
OPEN ACCESS

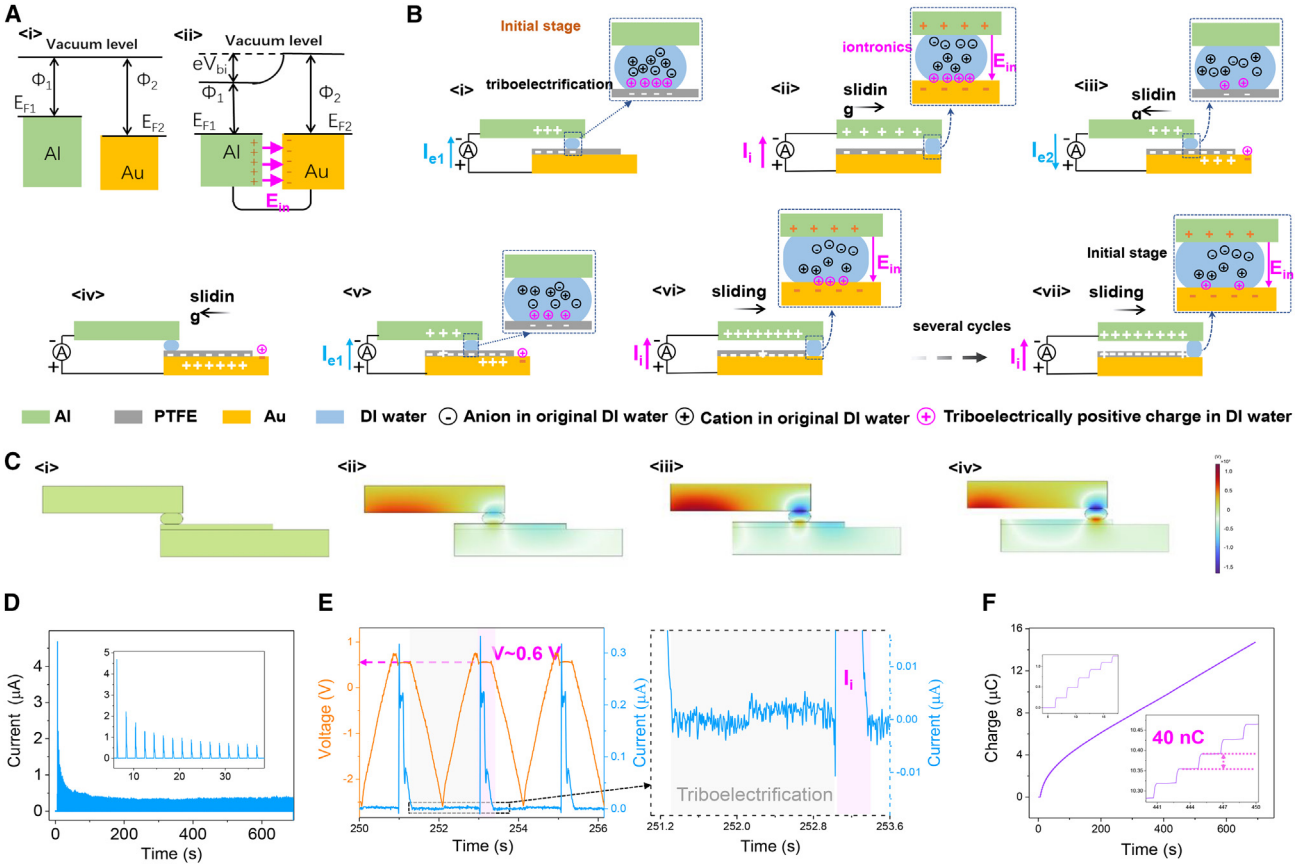

Figure 1. The working principle of triboiontronics

(A) The electron energy level of the aluminum (Al) and gold (Au) electrodes (i) before making contact and (ii) in thermodynamic equilibrium after circuit connection. EF1 and EF2 are the Fermi levels, and Φ1 and Φ2 are the work functions of the Al and Au, respectively. Vbi is the built-in voltage, and e in eVbi is the elementary charge.

(B) The working mechanism of triboiontronics.

(C) The COMSOL simulation of the triboelectric charging process of the sliding DI water droplet.

(D–F) The output (D) current, (E) voltage, and (F) charge of triboiontronics.

statically stayed between the Al and Au electrodes without triboelectrification, the discharging ionic DC current decayed very rapidly (Figure 2B, mulberry current). A higher ionic DC current (Figure 2B, blue current) was generated when the DI water droplet slid on the Au electrode. This was possible because the triboelectrification between water and Au promoted their interfacial charge transfer. In addition, a PTFE filter paper soaked with 20 μL of water was introduced to further investigate the synergy of triboelectrification and E_{in} during discharge (Figure 2C). The discharging DC current (Figure 2C, mulberry current) decayed rapidly when the device remained stationary. Once the Al electrode slid on the moist PTFE filter paper, each slide generated a pulse of discharging DC current (Figure 2C, blue current), and its discharge time became longer than that of the stationary state. The scanning electron microscopy (SEM) showed the porous structure of the PTFE filter paper, indicating its good ion permeability. The element fluorine was detected in the energy-dispersive spectrometry (EDS) analysis (Figure S4), which indicated an enhanced electron-accepting capability of the PTFE filter paper due to the stronger electron affinity of the fluorine element. An AC current was generated if the PTFE filter paper was dry when sandwiched between the Al and Au electrodes (Figure S5).

The output performance of a triboiontronics device depends on the triboelectrification, which can be regulated by the sliding distance, velocity, and solid-liquid contact area. On one hand, the longer the sliding distance, the higher the DC current that was generated due to the more triboelectric charges produced in the DI water droplet (Figure 2D). On the other hand, a slower sliding velocity was beneficial for improving the output DC current (Figure 2E), which might be because DI water had a better contact efficiency with PTFE, offering a longer discharge time with Au. It should be noted that the TTI device with two DI water droplets generated a higher DC current (~1 μA; Figure 2F) than that with one DI water droplet (~0.3 μA; Figure 1E), while their voltages were nearly the same (~0.6 V; Figure 2G). It indicated that E_{in} indeed originated from the work function difference. More convincing evidence is shown in Figures 2H and 2I, and the previous positive DC current as well as voltage became negative when the positions of the Al and Au electrodes were swapped. The DC current direction could be steered by the circuit connection of electrodes. Furthermore, such a rectification

Please cite this article in press as: Li et al., Transistor-like triboiontronics with record-high charge density for self-powered sensors and neurologic analogs, Device (2024), https://doi.org/10.1016/j.device.2024.100332

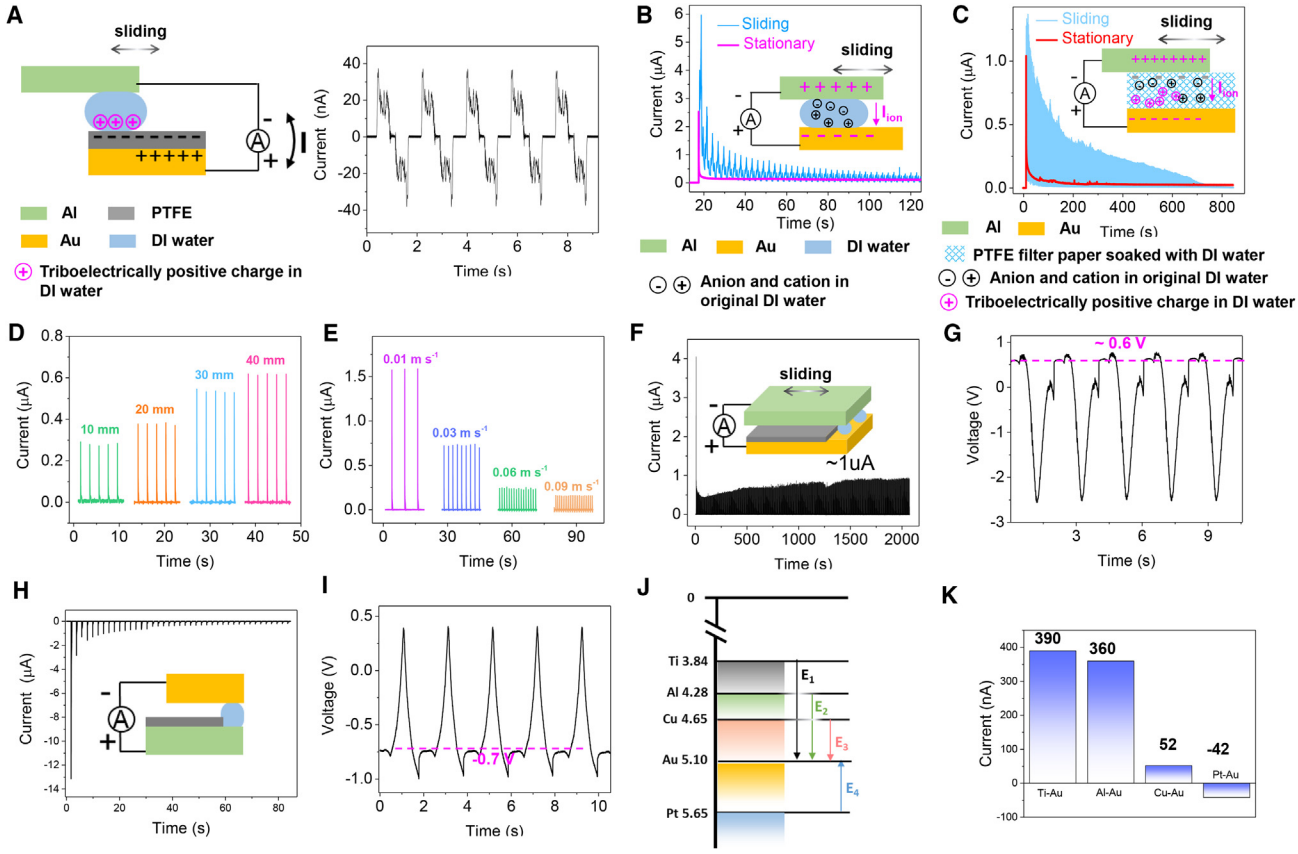

Figure 2. The output characteristics of triboiontronics

(A) The conventional structure of solid-liquid TENG and its output current.

(B) Comparison of the I_i generated by the work function difference in stationary and sliding mode.

(C) Comparison of the I_i generated through the coupling effect of triboelectrification and work function difference in stationary and sliding mode.

(D) The output current vs. sliding distance of the DI water droplet on the PTFE surface.

(E) The output current vs. sliding velocity of the DI water droplet on the PTFE surface.

(F and G) The (F) output current and (G) voltage of triboiontronics with two DI water droplets.

(H and I) The (H) output current and (I) voltage under the reverse E_{in}.

(J and K) The (J) work functions of different metals and their influence on the (K) output current of the triboiontronics device.

ionic DC current was not limited to the Au and Al electrodes but also applied to other metal pairs with different work functions; for example, Au and titanium (Ti) electrodes (Figure S6). The equivalent circuit of TTI devices in the discharge process is shown in Figure S7A, where the positively charged DI water was discharged under the E_{in} formed by the work function difference. The relationship between work function difference and output current could be inferred by the following equations.

First, the relationship between the charge and voltage of a capacitor is shown in the following formula:

$$Q = C \cdot (u - V_{bi}) \quad \text{(Equation 1)}$$

where Q is the charge of the capacitor, C is the equivalent capacitance, u is the output voltage, and $V_{bi} = \frac{\Phi_1 - \Phi_2}{e}$ is the built-in potential difference.

The formula for the output current is as follows:

$$i = \frac{dQ}{dt} = \frac{u}{R} \quad \text{(Equation 2)}$$

where R is the external resistance.

Therefore, u can be expressed as follows:

$$u = R\frac{d[C \cdot (u - V_{bi})]}{dt} \quad \text{(Equation 3)}$$

Here, the equivalent capacitance is approximated by a parallel plate capacitor:

$$C = \frac{\varepsilon_0 \varepsilon_r S}{d} \quad \text{(Equation 4)}$$

where ε_0 is the vacuum dielectric constant, ε_r the relative permittivity, d the thickness of the capacitor, and S the relative area of

Please cite this article in press as: Li et al., Transistor-like triboiontronics with record-high charge density for self-powered sensors and neurologic analogs, Device (2024), https://doi.org/10.1016/j.device.2024.100332

the capacitor (the area where the upper and lower electrodes face each other), which can be expressed as follows:

$$S = S_0 + At \quad \text{(Equation 5)}$$

where S_0 is the initial relative area between the two metal electrode plates , A is the sliding velocity (m^2/s), and t is the sliding time.

k is defined as

$$k = \frac{\varepsilon_0 \varepsilon_r}{d} \quad \text{(Equation 6)}$$

Thus, the capacitance can be expressed as follows:

$$C = k(S_0 + At) \quad \text{(Equation 7)}$$

Equation 3 evolved into

$$\frac{u}{R} = k(At + S_0) \cdot \frac{du}{dt} + kA(u - V_{bi}) \quad \text{(Equation 8)}$$

Equation 8 reads

$$\left(\frac{1}{R} - kA\right)u + V_{bi}kA = k(At + S_0)\frac{du}{dt} \quad \text{(Equation 9)}$$

which was integrated into the formula

$$\int_0^t \frac{dt}{k(At+S_0)} = \int_{U_0}^{U} \frac{du}{\left(\frac{1}{R} - kA\right)u + V_{bi}kA} \quad \text{(Equation 10)}$$

where U_0 is the potential difference of the original capacitor, and the ultimate result is as follows:

$$I = \frac{\left[\left(1+\frac{At}{S_0}\right)^{\frac{\frac{1}{R}-kA}{kA}} - 1\right]V_{bi}kA + \left(\frac{1}{R} - kA\right)\left(1+\frac{At}{S_0}\right)^{\frac{\frac{1}{R}-kA}{kA}}U_0}{1 - kAR} \quad \text{(Equation 11)}$$

where $\frac{1}{R} \gg kA$; thus, $\left(1+\frac{At}{S_0}\right)^{\frac{\frac{1}{R}-kA}{kA}} - 1 > 0$, and, therefore, it can be obtained from Equation 11 that I increases with the metal work function difference. The theoretically calculated output current of triboiontronics devices under various theoretical work function[20] differences (Figure 2J) is shown in Figure S7B. The current peak was gradually reduced with the decrease in the theoretical work functions difference between electrodes ($E_1 > E_2 > E_3$). The current direction even became negative under the reversed E_4 formed between the Au and platinum (Pt) electrodes. Moving from theory to experiment, the Au electrode was used as a reference electrode, and the counter electrode was altered to investigate the influence of work function differences on the amplitude and direction of output current. The experimental results (Figure 2K) were in good agreement with the theoretically calculated results (Figure S7B), with the parameters of $S_0 = 10^{-4}$ m^2, $A = 10^{-5}$ m^2 s^{-1}, $R = 10^8$ Ω, $k = 8.85 \times 10^{-9}$ F m^{-2}, $U_0 = 3 \times 10^{-5}$ V, and t = 0.0013 s. In comparison, the rectified I_i hardly appeared when the reference electrode and counter electrode were identical; i.e., using both Au or both Al (Figures S8 and S9). Such results were consistent with the systematic I-V curve when DI water droplet was sandwiched between identical electrodes (Figure S10).

The sliding mode of triboiontronics demonstrated its rectifying function through the synergy of triboelectrification and work function difference. Inspired by the evolution of multifunctional electronics from transistors and the subsequent integration, we proposed TTI, in which the Al, Au, and triboelectrically charged DI water were analogous to the function of source, drain, and gate terminals. Two more Al back electrodes under fluorinated ethylene propylene (FEP) could produce an AC due to electrostatic induction (Figures 3A and S11), and the source-drain terminal could directly generate a DC current (Figure 3B). The single DI water droplet was triboelectrically charged by mechanical vibration, and its charges would be released to form a DC current upon the source-drain terminal, as shown in Figure 3C. Similar to the traditional transistor, TTI also offers possibilities for various structural designs and can regulate its output performance. As shown in Figure S12, the DI water droplet slid on the FEP at different heights to the junction of the source-drain terminal. These results indicated that the DI water droplet carried different triboelectric charges through controlling the sliding distance that could regulate the output current. As shown in Figure 3D, the narrower the gap between the source and drain terminals, the greater the DC current generated as the stronger E_{in} would be formed to promote the I_i. Increasing the volume of the DI water droplet not only improved its triboelectric charges but also increased the contact area between the water droplet and the source-drain terminal, enhancing the output DC current (Figure 3E). The increasing trend of output DC current became unapparent when the width of source-drain charge-collecting terminals was increased to 10 cm (Figure 3F). This might be caused by the influence from more hydrophilic metal surfaces when the water droplet passed through, affecting the interfacial wettability. The output charges and voltages of TTI devices with different parameters are shown in Figure S13. A photograph of a TTI device with a gap of 500 μm, volume of 100 μL, and width of 5 mm is shown in Figure S14. Its average charge transfer reached a value of 0.700 μC, and the contact area of the DI water droplet was 0.503 cm^{-2}. Therefore, a record-high charge density of 13.926 mC m^{-2} was obtained in this work (Figure 3G), which was an order of magnitude higher than those from the state-of-art devices reported

Please cite this article in press as: Li et al., Transistor-like triboiontronics with record-high charge density for self-powered sensors and neurologic analogs, Device (2024), https://doi.org/10.1016/j.device.2024.100332

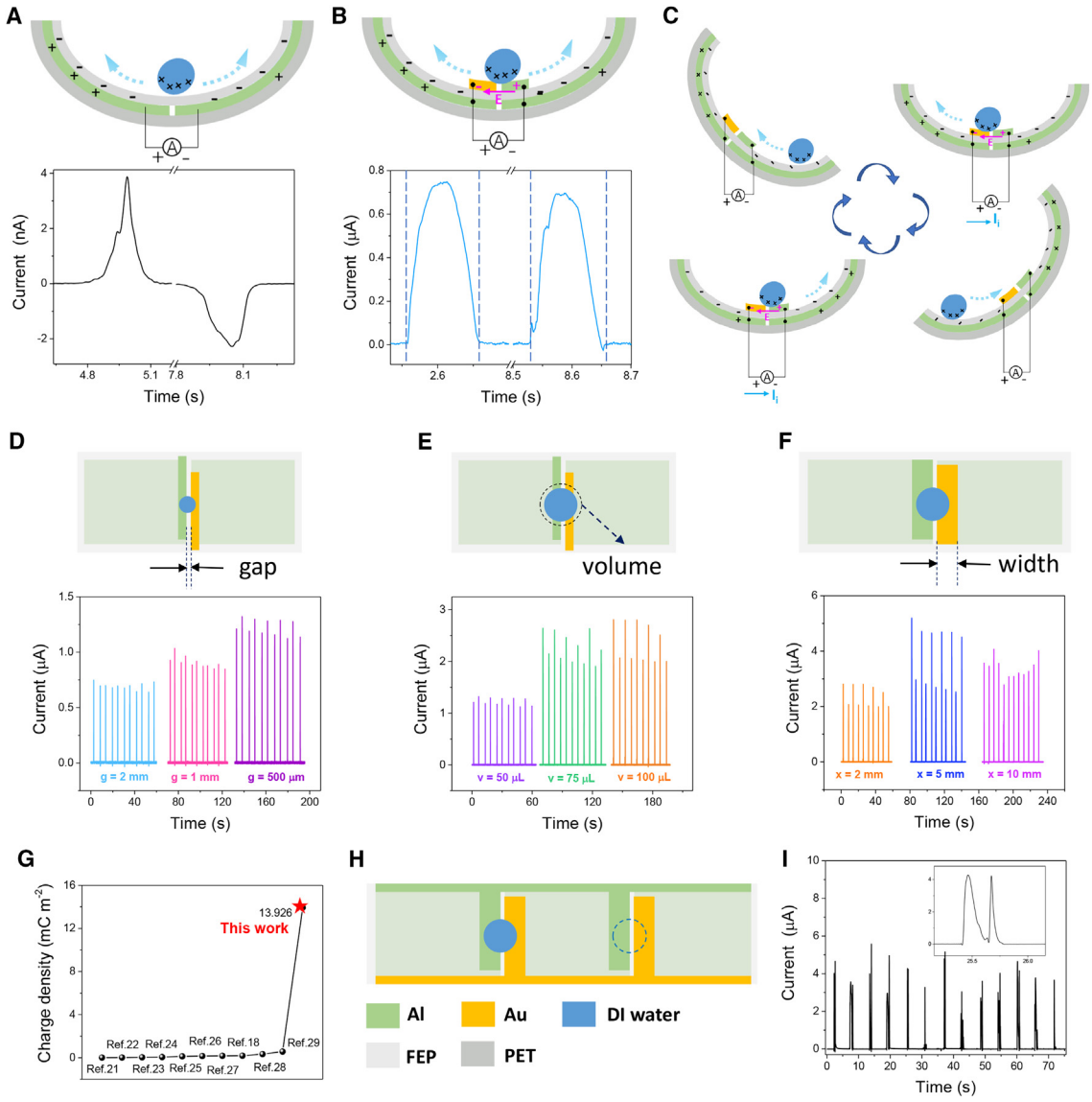

Figure 3. The design of the TTI device

(A) Structure and current signal of the free-standing TENG.

(B) Structure and current signal of the TTI device.

(C) The working mechanism of the TTI device.

(D–F) The structural designability of the TTI device in the gap of the source-drain terminal, the volume of the DI water droplet, and the width of the electrode, and its corresponding output current.

(G) Comparison of charge density in previous studies[18,21–29] and in our work.

(H and I) Structure schematic of the TTI device with two source-drain terminals (H) and its output current (I).

so far (from 0.014 to 0.566 mC/m^2).[18,21–29] The limited electron-accepting/donating and charge-storing capability of solid dielectric surfaces during CE was the main challenge for further improving the charge density of conventional solid-liquid TENGs. Despite DEGs promoting their output through the direct contact between the charged water droplet and electrode, they only harvest part of the charges from water droplets by one of the electrodes and are still restrained by the limitation of a solid dielectric surface. In contrast, the record-high charge density of the TTI device benefitted not only from the direct contact between the charged water and electrodes but also from the fast migration of charges driven by E_{in}. More importantly, the single water droplet in the TTI device could be repeatedly charged (slid on the dielectric layer) and discharged (positioned on the source-drain terminal). As shown in Figures 3H and 3I, two DC signals were generated when the DI water droplet slid on two source-drain terminals in sequence after triboelectrification with FEP. The TTI device did not require water drops falling continuously from a certain height, as reported

Please cite this article in press as: Li et al., Transistor-like triboiontronics with record-high charge density for self-powered sensors and neurologic analogs, Device (2024), https://doi.org/10.1016/j.device.2024.100332

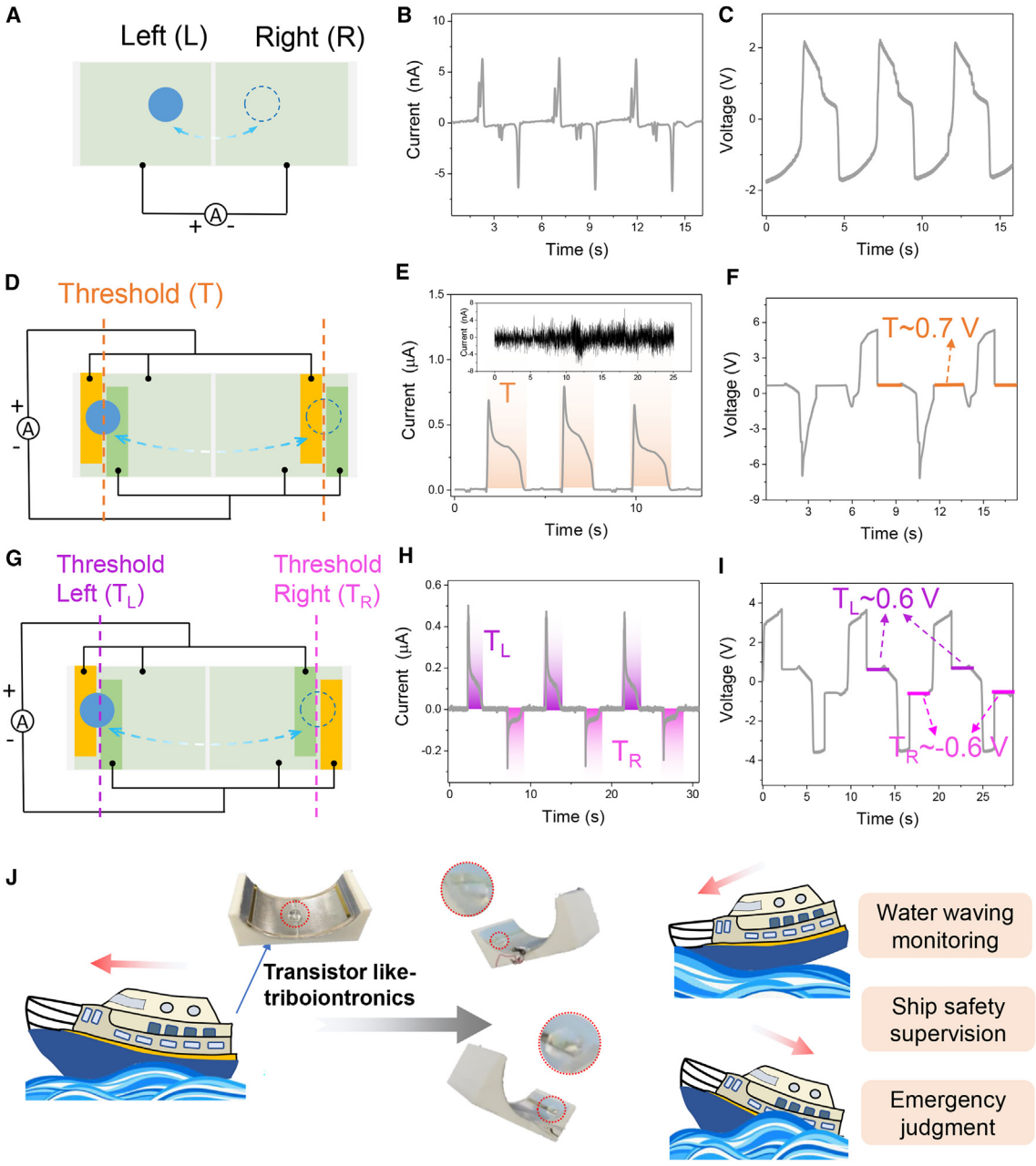

Figure 4. The threshold-monitoring function of the TTI device

(A–C) Traditional freestanding TENG (A) and its output (B) current and (C) voltage.

(D–F) A TTI device as a self-powered threshold sensor (D) and its output (E) current and (F) voltage.

(G–I) A TTI device for left/right self-powered threshold sensing (G) and its output (H) current and (I) voltage.

(J) The potential application of a TTI device in self-powered threshold monitoring.

previously,[34–36] thus expanding its application scenarios for both energy harvesting and information sensing.

Vibration movement could be monitored by a water droplet TENG[26] with freestanding mode (Figure 4A), benefitting from the smaller friction resistance of the single DI water droplet on FEP. However, the AC-sensing signals (Figures 4B and 4C) of conventional TENGs[26] are small and easily affected by the environment, resulting in a low SNR due to the nanolevel of current and limited accuracy in some vector threshold sensors. For TTI, once the DI water droplet moved to one of the source-drain terminals, a DC threshold-sensing signal responded (Figures 4D and 4E). The orange part in Figure 4E indicates the residence time of the water droplet on the source-drain terminal. At the same time, the voltage became approximately 0.7 V, which mainly

Please cite this article in press as: Li et al., Transistor-like triboiontronics with record-high charge density for self-powered sensors and neurologic analogs, Device (2024), https://doi.org/10.1016/j.device.2024.100332

originated from the work function difference of the source-drain terminal (Figure 4F, orange line). Such a microlevel current output generated by TTI provided a high SNR as a more accurate method to monitor the vibration movements. The SNR is an important parameter for sensors defined by the strength of the desired signal compared with the undesired background noise, In the formula[37,38]

$$SNR = 20 \cdot \lg \frac{I_{Signal}^{RMS}}{I_{Noise}^{RMS}} \quad \text{(Equation 12)}$$

I_{Signal}^{RMS} is the root-mean-square (RMS) of the output current signal, and I_{Noise}^{RMS} is the RMS of the noise signal. Considering that the RMS value of the noise signal was 1.563 nA (Figure 4E, inset), the SNR ratio related to TTI was calculated to be 53.217 dB, which was almost 3 times that of a freestanding TENG (19.854 dB). Such high SNR of TTI offered a significant character for self-powered sensors. As shown in Figures 4G and 4H, a positive current was generated when the DI water droplet moved to the left source-drain terminal (the left threshold [T_L]). On the contrary, a negative current was generated when the DI water droplet moved to the right source-drain terminal (the right threshold [T_R]). Moreover, the positive and negative constant voltage (about ~0.6 V) could also be used to distinguish the direction of vibrational movement (Figure 4I). Therefore, the TTI has huge potential for detection of ship movement. Figure 4J shows the gated DI water droplet at the neutral position in a balanced situation. The DI water droplet would move to different source-drain terminals during a bump of the ship, and its negative or positive threshold-sensing signals present the specific moving direction, amplitude, and frequency of the ship (Video S1). The characteristics of a high SNR from TTI provide a more accurate and rapid response and might serve as self-powered threshold sensors for alarm and warning systems, such as for shipwrecks, driving collisions, earthquakes and bridge/tunnel collapse. More movement information, such as the specific threshold position, could be also obtained through the optimized design of source-drain terminals. Furthermore, as one type of iontronics, TTI is almost unaffected by magnetic fields, which could extend its application in broader scenarios.

In practice, vibrational movement is more complex, especially when its vibrational equilibrium position deviates from the initial position. For example, the rearmost part of a ship is constantly impacted by waves, making its center of gravity shift to the bow, thus causing an imbalance in the entire ship. A TTI device with the function of a multilevel threshold was proposed to alert during some emergencies, and different threshold positions were presented via four source-drain terminals. Figures 5A and 5B depict the structure of such a multifunctional TTI device as side and top views, and photographs are also shown in Figure S15. Different sensing electrical signals of a multifunctional TTI device were produced when the DI water droplet moved to different positions (Figures S16 and S17). Namely, the electrical signal in one period corresponded to each movement trajectory of the DI water droplet. It can be seen in Figures 5C–5E that the positive and negative sensing signals were generated with symmetrical numbers, which indicated that the vibration center of gravity of the multifunctional TTI was at the horizontal center. Moreover, even-numbered sensing signals in the same direction were produced when the position of the DI water droplet was in between the T_1 and T_2 (Figure 5D). The odd-numbered sensing signals in the same direction presented the DI water droplet exactly moved to the position of one source-drain terminal, as shown in Figures 5A and 5C. Furthermore, the more symmetrical sensing signals appeared, the larger the vibration amplitude of the DI water droplet became. Such signals indicated that the object was experiencing severe turbulence in both directions. On the other hand, the decreasing amount of positive sensing signals (Figures 5F–5H) indicated that the center of gravity of the DI water droplet gradually trended to the right side, which further explained that the object was in a very unbalanced state. The practical movement trajectories of the DI water droplet are shown in Figures S16 and S17.

TTI self-powered sensors have very powerful functions and huge potential for various sensing applications in which the electric signal characteristics are closely related to the physical stage of the DI water droplet. Furthermore, TTI could also be used to build logic analogy for information transmission and human-machine interaction interfaces. As shown in the photograph (Figure 6A) and circuit diagram (Figure 6B), the left DI water droplet slid from FEP as a gate terminal, forming a clockwise (positive) current loop in the left circuit. Vice versa, the counter-clockwise (negative) current loop was generated in the right circuit, when the right DI water droplet connected to the right source-drain terminal. The positive current as a command signal could be also transmitted to the robotic circuit controller for raising the left leg of a robot (Figure 6Ci). Once the gate DI water droplet was absorbed by dust-free paper, the connection of the source-drain terminal was broken, the current decreased to zero, and the robot returned to its initial state (Figure 6Cii). Similarly, the negative current generated by the gate of the right DI water droplet controlled the movement of the right leg of the robot (Figure 6Ciii). The brain controls the body's movement of walking through accurate transmission of information from the central nervous system via the neurologic circuit for the coordinated motion of the lower limbs.[9] A TTI device could enable a neurologic circuit to control robotic movements in a similar way with and low power consumption (Video S2). Parameters influencing TTI, such as work function difference/gap of electrodes and friction distance/velocity of the water droplet, are shown in Figure 6D. Besides, surface modification of the solid, application of non-evaporable liquid droplet,[39] as well as device encapsulation are good ways to improve the feasibility and stability of TTI.

Conclusion

Electronics are currently approaching the limit of Moore's law. Inspired by the information transmission in neuron systems, iontronics provide an alternative approach to improve the energy and information flow. However, the regulation of charges in iontronics is a long-lasting challenge. In this work, a mechano-driven TTI was proposed through the synergy of triboelectrification at the solid-liquid interface and work function difference between dissimilar metal electrodes. After charging by friction against the solid dielectric, the triboelectrically charged DI water droplet would be discharged under the constant E_{in}

Please cite this article in press as: Li et al., Transistor-like triboiontronics with record-high charge density for self-powered sensors and neurologic analogs, Device (2024), https://doi.org/10.1016/j.device.2024.100332

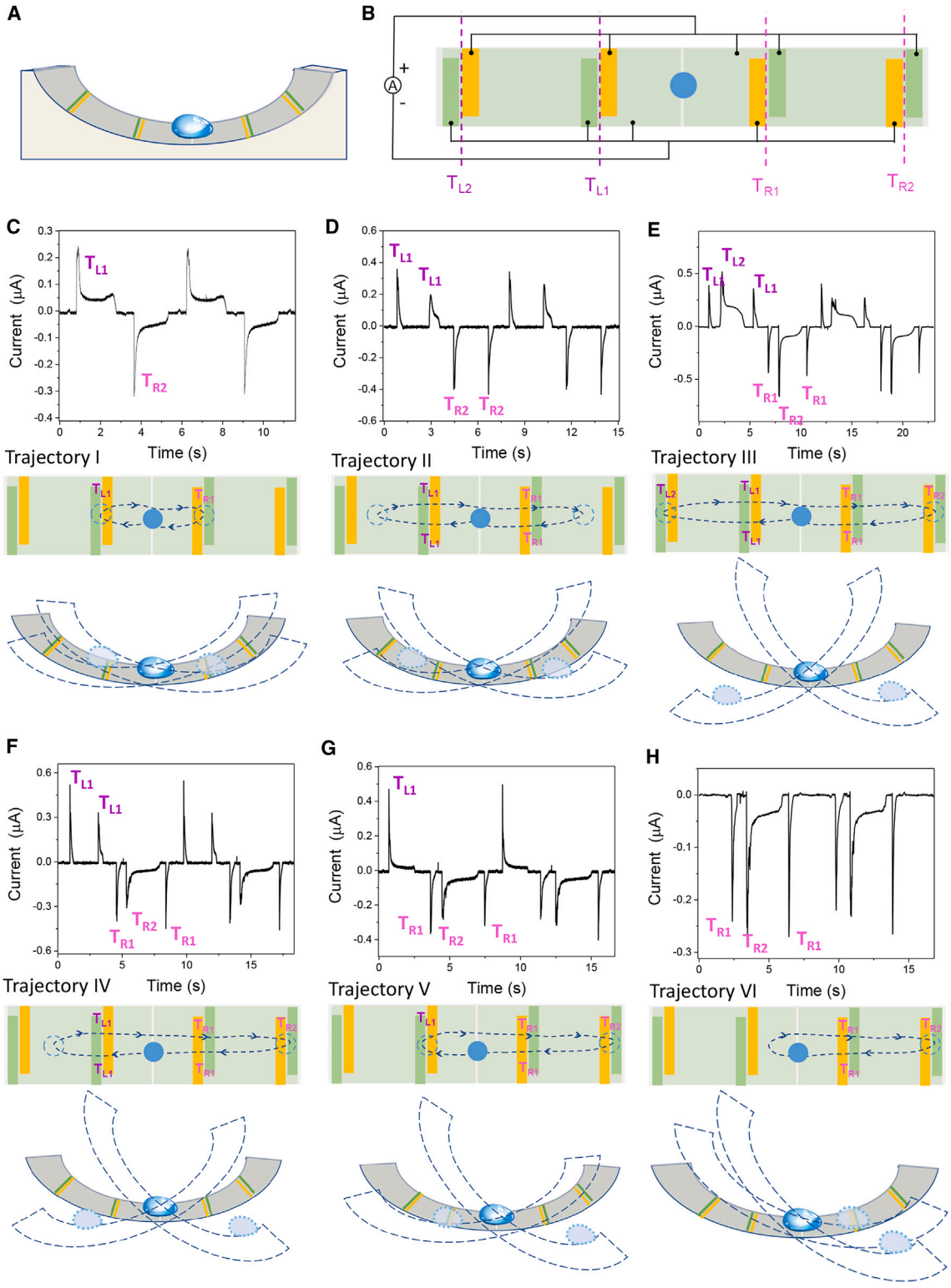

Figure 5. The self-powered sensor based on TTI

(A and B) Side view (A) and top view (B) of a TTI self-powered sensor with the multilevel threshold.

(C–E) A TTI self-powered sensor under the different symmetrical movement trajectories of the DI water droplet gate.

(F–H) A TTI self-powered sensor under asymmetrical movement trajectories of the DI water droplet gate (to the right side).

Please cite this article in press as: Li et al., Transistor-like triboiontronics with record-high charge density for self-powered sensors and neurologic analogs, Device (2024), https://doi.org/10.1016/j.device.2024.100332

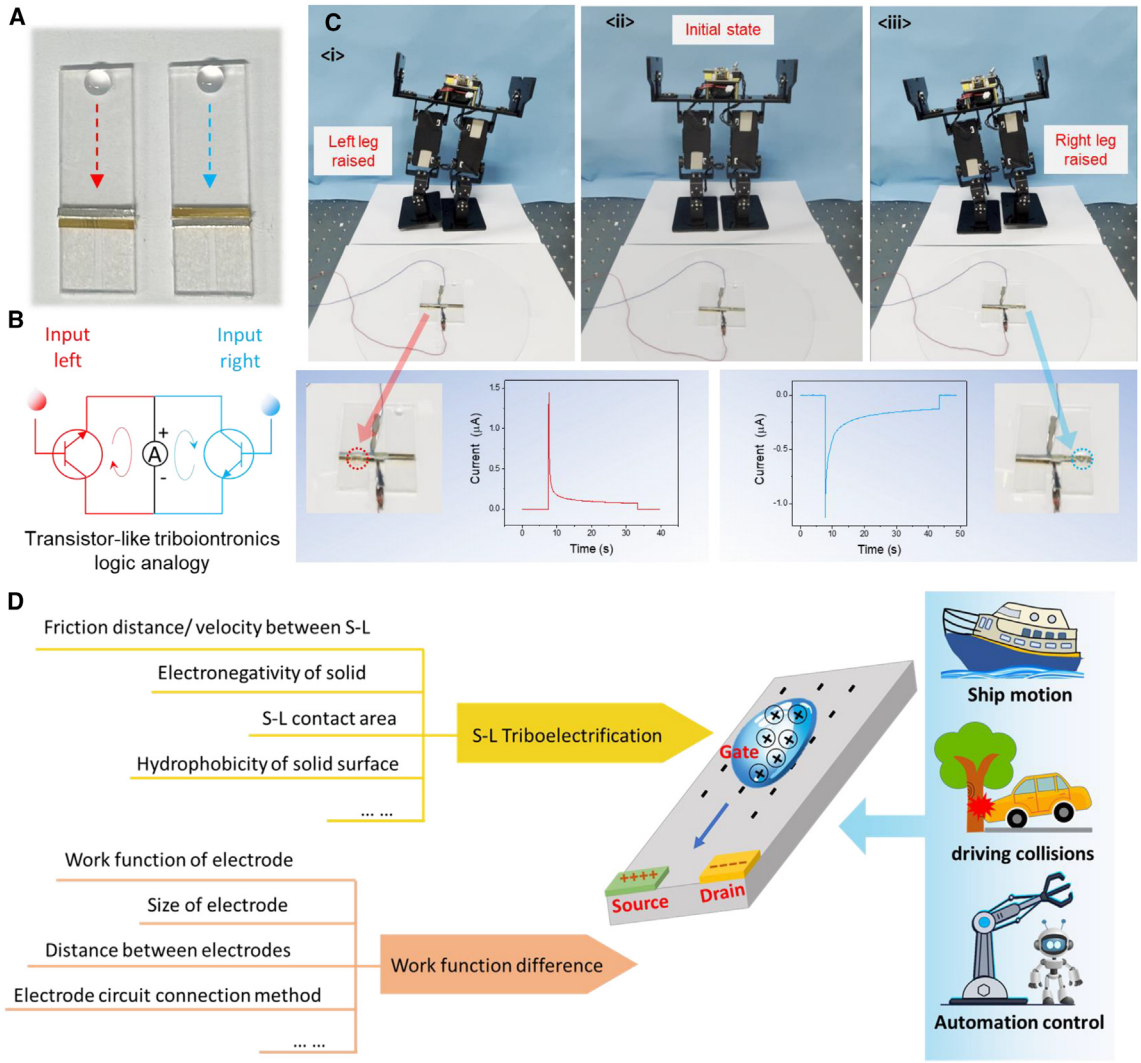

Figure 6. Control of an neurologic analog circuit by a TTI device

(A) Photograph of two TTI devices.

(B) The neurologic analog circuit of the TTI device.

(C) The robotic movements controlled by the TTI device.

(D) Influencing parameters and potential applications of TTI devices.

formed by the work function difference. Its transferred charge density set a record of 13.926 mC/m^2, which was an order of magnitude higher than those from the state-of-art devices reported so far (from 0.014 to 0.566 mC/m^2).[18,21–29] A high SNR was obtained for mechano-driven, gate-tunable TTI, and it showed great potential for self-powered threshold sensors. As one type of iontronics, TTI is almost unaffected by magnetic fields, which could extend its application scenarios. This work enables the possibility to tune mechano-driven current signals, which could not only be used as self-powered sensors, but also work as a neurologic analog circuit to control robot movements. We envision that TTI will open up avenues for many applications in the near future, from scavenging energy and building neuromorphic integrated circuits to developing low-power, in-sensor computing.

EXPERIMENTAL PROCEDURES

Resource availability

Lead contact

Requests for further information, resources, and reagents should be directed to and will be fulfilled by the lead contact, Di Wei (weidi@binn.cas.cn).

Materials availability

The materials generated in this study are available from the lead contact upon reasonable request.

Data and code availability

The data used to support the findings of this study are available from the lead contact upon reasonable request.

The fabrication of the triboiontronics

The triboiontronics device consisted of two different metal materials, an electret material, a DI water droplet, and hard base supporting materials. First, two different metal materials (an Au film and Al film) were attached to two acrylic

plates. The Au film was fabricated by magnetron sputtering technology (Discovery635). Then, one of the metal surfaces was attached by an electret material (such as FEP or PTFE) that served as the triboelectrification layer and remained an exposed area. Furthermore, a DI water droplet was sandwiched between one metal and triboelectrification layer at the initial movement. The movement of the DI water droplet on the surface of one metal and triboelectrification layer was driven by a linear motor (LinMot BF01-37).

The fabrication of the TTI device

The TTI consisted of two metal materials, an electret material, a DI water droplet, and soft base supporting materials. First, two identical metal materials were attached to the surface of the soft base supporting materials (such as polyester film) at a certain distance. Then, the entire soft base support material and the two identical metals were covered with an electret material (such as FEP or PTFE) that served as a triboelectric layer. Next, two different metal materials (such as Au film and Al film) were attached to the surface of the electret material, keeping a certain gap between each other. Furthermore, the whole device was fixed on a curved support mold that was printed by three-dimensional printer (RAISE 3D), and a DI water droplet vibrated back and forth on this device through a customized swing mechanical structure.

The electrical characteristics measurement

A programmable electrometer (Keithley Instruments, model 6514) was used to measure the current, voltage, and charge signal of TTI. The theoretical model was simulated by COMSOL software.

SUPPLEMENTAL INFORMATION

Supplemental information can be found online at https://doi.org/10.1016/j.device.2024.100332.

ACKNOWLEDGMENTS

This work was supported by the Beijing Natural Science Foundation (grant IS23040).

AUTHOR CONTRIBUTIONS

S.L., D.W., and Z.L.W. contributed to the research conceptualization and methodology, conducted the experimental validation, and wrote the original manuscript. Z.Z. and M.W. contributed to theoretical calculations. P.P. contributed to the measurement of SEM and EDX, and X.L. contributed to the fabrication of the TENG. F.Y., Y.D., and Q.Z. contributed to software programming. All authors discussed the results and commented on the manuscript.

DECLARATION OF INTERESTS

The authors declare no competing interests.

Received: January 31, 2024
Revised: February 22, 2024
Accepted: March 6, 2024
Published: April 5, 2024

REFERENCES

1. Wu, J., Shen, Y.-L., Reinhardt, K., Szu, H., and Dong, B. (2013). A Nanotechnology Enhancement to Moore's Law. Applied Computational Intelligence and Soft Computing, 426962. https://doi.org/10.1155/2013/426962.
2. Warren, P. (2004). The future of computing-new architectures and new technologies. IEE Proc. - Nanobiotechnol. *151*, 1–9. https://doi.org/10.1049/IP-NBT%3A20030876.
3. Wei, D., Yang, F., Jiang, Z., and Wang, Z. (2022). Flexible iontronics based on 2D nanofluidic material. Nat. Commun. *13*, 4965. https://doi.org/10.1038/s41467-022-32699-x.
4. Qian, H., Wei, D., and Wang, Z. (2023). Bionic iontronics based on nano-confined structures. Nano Res. *16*, 11718–11730. https://doi.org/10.1007/s12274-023-5705-z.
5. Yu, L., Li, X., Luo, C., Lei, Z., Wang, Y., Hou, Y., Wang, M., and Hou, X. (2023). Bioinspired nanofluidic iontronics for brain-like computing. Nano Res. *17*, 503–514. https://doi.org/10.1007/s12274-023-5900-y.
6. Sabbagh, B., Fraiman, N.E., Fish, A., and Yossifon, G. (2023). Designing with iontronic logic gates from a single polyelectrolyte diode to an integrated ionic circuit. ACS Appl. Mater. Interfaces *15*, 23361–23370. https://doi.org/10.1021/acsami.3c00062.
7. Xing, Y., Zhou, M., Si, Y., Yang, C.-Y., Feng, L.-W., Wu, Q., Wang, F., Wang, X., Huang, W., Cheng, Y., et al. (2023). Integrated opposite charge grafting induced ionic-junction fiber. Nat. Commun. *14*, 2355. https://doi.org/10.1038/s41467-023-37884-0.
8. Kim, H.J., Chen, B., Suo, Z., and Hayward, R.C. (2020). Ionoelastomer junctions between polymer networks of fixed anions and cations. Science *367*, 773–776. https://doi.org/10.1126/science.aay8467.
9. Li, X., Li, S., Guo, X., Shao, J., Wang, Z.L., and Wei, D. (2023). Triboiontronics for efficient energy and information flow. Matter *6*, 3912–3926. https://doi.org/10.1016/j.matt.2023.08.022.
10. Nie, J., Ren, Z., Xu, L., Lin, S., Zhan, F., Chen, X., and Wang, Z.L. (2020). Probing contact-electrification-induced electron and ion transfers at a liquid-solid interface. Adv. Mater. *32*, e1905696. https://doi.org/10.1002/adma.201905696.
11. Wang, Z.L., and Wang, A.C. (2019). On the origin of contact-electrification. Mater. Today *30*, 34–51. https://doi.org/10.1016/j.mattod.2019.05.016.
12. Sun, M., Lu, Q., Wang, Z.L., and Huang, B. (2021). Understanding contact electrification at liquid-solid interfaces from surface electronic structure. Nat. Commun. *12*, 1752. https://doi.org/10.1038/s41467-021-22005-6.
13. Lin, S., Chen, X., and Wang, Z.L. (2022). Contact electrification at the liquid-solid interface. Chem. Rev. *122*, 5209–5232. https://doi.org/10.1021/acs.chemrev.1c00176.
14. Willatzen, M., Voon, L., and Wang, Z.L. (2020). Quantum theory of contact electrification for fluids and solids. Adv. Funct. Mater. *30*, 1910461. https://doi.org/10.1002/adfm.201910461.
15. Lin, S., Xu, L., Chi Wang, A., and Wang, Z.L. (2020). Quantifying electron-transfer in liquid-solid contact electrification and the formation of electric double-layer. Nat. Commun. *11*, 399. https://doi.org/10.1038/s41467-019-14278-9.
16. Li, Y., Qin, X., Feng, Y., Song, Y., Yi, Z., Zheng, H., Zhou, P., Wu, C., Yang, S., Wang, L., et al. (2024). A droplet-based electricity generator incorporating Kelvin water dropper with ultrahigh instantaneous power density. Droplet *3*, e91. https://doi.org/10.1002/dro2.91.
17. Xu, W., Zheng, H., Liu, Y., Zhou, X., Zhang, C., Song, Y., Deng, X., Leung, M., Yang, Z., Xu, R.X., et al. (2020). A droplet-based electricity generator with high instantaneous power density. Nature *578*, 392–396. https://doi.org/10.1038/s41586-020-1985-6.
18. Xu, X., Li, P., Ding, Y., Xu, W., Liu, S., Zhang, Z., Wang, Z., and Yang, Z. (2022). Droplet energy harvesting panel. Energy Environ. Sci. *15*, 2916–2926. https://doi.org/10.1039/d2ee00357k.
19. Wang, H.L., Zhang, B., Chen, T., Mao, W., and Wang, Y. (2023). High-efficiency single-droplet energy harvester for self-sustainable environmental intelligent networks. Adv. Energy Mater. *13*, 2302858. https://doi.org/10.1002/aenm.202302858.
20. Sze, S.M., and Ng, K.K. (2007). Physics of Semiconductor Devices (John Wiley & Sons). https://doi.org/10.1002/0470068329.
21. Zhao, L., Liu, L., Yang, X., Hong, H., Yang, Q., Wang, J., and Tang, Q. (2020). Cumulative charging behavior of water droplet driven freestanding triboelectric nanogenerators toward hydrodynamic energy harvesting. J. Mater. Chem. A *8*, 7880–7888. https://doi.org/10.1039/d0ta01698e.
22. Xu, W., Li, X., Brugger, J., and Liu, X. (2022). Study of the enhanced electricity output of a sliding droplet-based triboelectric nanogenerator for

droplet sensor design. Nano Energy *98*, 107166. https://doi.org/10.1016/j.nanoen.2022.107166.

23. Meng, J., Zhang, L., Liu, H., Sun, W., Wang, W., Wang, H., Yang, D., Feng, M., Feng, Y., and Wang, D. (2023). A new single-electrode generator for water droplet energy harvesting with a 3 mA current output. Adv. Energy Mater. *14*. https://doi.org/10.1002/aenm.202303298.
24. Yang, L., Yu, J., Guo, Y., Chen, S., Tan, K., and Li, S. (2023). An electrode-grounded droplet-based electricity generator (EG-DEG) for liquid motion monitoring. Adv. Funct. Mater. *33*, 2302147. https://doi.org/10.1002/adfm.202302147.
25. Wu, H., Mendel, N., van der Ham, S., Shui, L., Zhou, G., and Mugele, F. (2020). Charge trapping-based electricity generator (CTEG): an ultrarobust and high efficiency nanogenerator for energy harvesting from water droplets. Adv. Mater. *32*, e2001699. https://doi.org/10.1002/adma.202001699.
26. Wei, X., Zhao, Z., Zhang, C., Yuan, W., Wu, Z., Wang, J., and Wang, Z.L. (2021). All-weather droplet-based triboelectric nanogenerator for wave energy harvesting. ACS Nano *15*, 13200–13208. https://doi.org/10.1021/acsnano.1c02790.
27. Xie, L., Yin, L., Liu, Y., Liu, H., Lu, B., Zhao, C., Khattab, T.A., Wen, Z., and Sun, X. (2022). Interface engineering for efficient raindrop solar cell. ACS Nano *16*, 5292–5302. https://doi.org/10.1021/acsnano.1c10211.
28. Kuang, H., Huang, S., Zhang, K., Xu, L., Cai, X., Zhang, C., Chen, J., Li, Y., Wang, X., Jin, H., et al. (2023). Generating direct current electricity from ionic droplets by using ferroelectric material. ACS Energy Lett. *8*, 3832–3838. https://doi.org/10.1021/acsenergylett.3c01381.
29. Zhang, Q., Li, Y., Cai, H., Yao, M., Zhang, H., Guo, L., Lv, Z., Li, M., Lu, X., Ren, C., et al. (2021). A single-droplet electricity generator achieves an ultrahigh output over 100 V without pre-charging. Adv. Mater. *33*, e2105761. https://doi.org/10.1002/adma.202105761.
30. Vilitis, O., Rutkis, M., Busenberg, J., and Merkulov, D. (2016). Determination of contact potential difference by the kelvin probe (Part I) I. basic principles of measurements. Latv. J. Phys. Tech. Sci. *53*, 48–57. https://doi.org/10.1515/lpts-2016-0013.
31. Varpula, A., Laakso, S.J., Havia, T., Kyynäräinen, J., and Prunnila, M. (2014). Harvesting vibrational energy using material work functions. Sci. Rep. *4*, 6799. https://doi.org/10.1038/srep06799.
32. Varpula, A., Laakso, S.J., Havia, T., Kyynäräinen, J., and Prunnila, M. (2014). Contacting mode operation of work function energy harvester. J. Phys, Conf. Ser. *557*, 012010. https://doi.org/10.1088/1742-6596/557/1/012010.
33. Kuehne, I., Frey, A., Marinkovic, D., Eckstein, G., and Seidel, H. (2008). Power MEMS—a capacitive vibration-to-electrical energy converter with built-in voltage. Sens. Actuators A Phys. *142*, 263–269. https://doi.org/10.1016/j.sna.2007.02.036.
34. Peng, J., Zhang, L., Sun, W., Liu, Y., Yang, D., Feng, M., Feng, Y., and Wang, D. (2022). High-efficiency droplet triboelectric nanogenerators based on arc-surface and organic coating material for self-powered anti-corrosion. Appl. Mater. Today *29*, 101564. https://doi.org/10.1016/j.apmt.2022.101564.
35. Zheng, Y., Li, J., Xu, T., Cui, H., and Li, X. (2023). Triboelectric nanogenerator for droplet energy harvesting based on hydrophobic composites. Materials *16*, 5439. https://doi.org/10.3390/ma16155439.
36. Zhang, H., Yin, K., Wang, L., Deng, Q., He, Y., Xiao, Z., Li, G., and Dai, G. (2023). A robust droplet triboelectric nanogenerator with self-cleaning ability achieved by femtosecond laser. ACS Appl. Mater. Interfaces *15*, 30902–30912. https://doi.org/10.1021/acsami.3c01864.
37. Wang, Z., An, J., Nie, J., Luo, J., Shao, J., Jiang, T., Chen, B., Tang, W., and Wang, Z.L. (2020). A self-powered angle sensor at nanoradian-resolution for robotic arms and personalized medicare. Adv. Mater. *32*, 2001466. https://doi.org/10.1002/adma.202001466.
38. Box, G. (1988). Signal-to-noise ratios, performance criteria, and transformations. Technometrics *30*, 1–17. https://doi.org/10.2307/1270311.
39. Qin, H., Xu, L., Zhan, F., and Wang, Z.L. (2023). Electron transfer induced contact-electrification at oil and oleophobic dielectric interface. Nano Energy *116*, 108762. https://doi.org/10.1016/j.nanoen.2023.108762.